Journal of Power Sources 216 (2012) 139–144

Contents lists available at SciVerse ScienceDirect

Journal of Power Sources

journal homepage: www.elsevier.com/locate/jpowsour

A comparison of sputtered and mechanically milled Cu_6Sn_5 + C materials for Li-ion battery negative electrodes

J.S. Thorne [a], J.R. Dahn [a,b,c,d], M.N. Obrovac [a,b,c], R.A. Dunlap [a,b,e,*]

[a] Department of Physics and Atmospheric Science, Dalhousie University, P.O. Box 15000, Halifax, Nova Scotia B3H 4R2, Canada
[b] Institute for Research in Materials, Dalhousie University, P.O. Box 15000, Halifax, Nova Scotia B3H 4R2, Canada
[c] Department of Chemistry, Dalhousie University, P.O. Box 15000, Halifax, Nova Scotia B3H 4R2, Canada
[d] Department of Process Engineering and Applied Science, Dalhousie University, P.O. Box 15000, Halifax, Nova Scotia B3H 4R2, Canada
[e] College of Sustainability, Dalhousie University, P.O. Box 15000, Halifax, Nova Scotia B3H 4R2, Canada

HIGHLIGHTS

- Electrochemical cycling characteristics of nanostructured Sn–Cu–C are reported.
- The study provides a systematic comparison of sputtered and milled samples.
- Microstructural changes during cycling are investigated.
- Results help to understand cycling behavior of commercial Sn-based anodes.
- Provides insight into reactions in commercially viable CuSn-based materials.

ARTICLE INFO

Article history:
Received 22 February 2012
Received in revised form
22 May 2012
Accepted 23 May 2012
Available online 30 May 2012

Keywords:
Cu_6Sn_5
Sn–Cu–C
Li-ion batteries
Mechanical milling
Nanostructured materials

ABSTRACT

$Sn_{27}Cu_{33}C_{40}$ produced by mechanical milling is compared with $Sn_{27}Cu_{31}C_{42}$ and $Sn_{26}Cu_{31}C_{43}$ produced by magnetron sputtering for use as anode materials in Li-ion batteries. The sputtered samples were found to be amorphous/nanostructured and had a greater degree of atomic intermixing in comparison to the milled sample, which was more crystalline. Samples were incorporated as electrodes in Li-half cells and had a capacity of about 400 mAh g^{-1}. Significant capacity loss was observed beginning near the 50th cycle for the mechanically milled sample, while little capacity loss was observed for the sputtered samples after 100 cycles. Despite its good cycling performance, amorphous Cu_6Sn_5 + C was found to crystallize as Li is cycled, resulting in the aggregation of Cu_6Sn_5 grains. Structural changes during lithiation and delithiation as well as the evolution of the electrochemistry are compared and contrasted for the two materials.

© 2012 Elsevier B.V. All rights reserved.

1. Introduction

Nanostructured Sn containing materials are considered as candidates for negative electrode materials for next generation Li-ion batteries. This is due to their high theoretical specific and volumetric capacity (i.e. 993 mAh g^{-1}, 2111 mAh cm^{-3} for Sn, including volume expansion, compared to 372 mAh g^{-1}, 744 mAh cm^{-3} for graphite). However, alloy materials can suffer from poor charge–discharge cycle life caused by high volume changes associated with lithiation and delithiation [1]. Of the tin-transition metal (TM) carbon alloys, Sn–Co–C-based materials [2] have been commercialized by Sony. However, Co is an expensive raw material and other alternatives or substitution of other transition metals for Co are being considered [3].

Copper is a possible candidate for replacing or lowering the Co content by substitution in Sn–Co–C alloys. At the present time, the cost of Cu by weight is about one-fourth the price of Co (www.metalprices.com). Numerous studies have been reported on the Sn–Cu system, with particular emphasis on Cu_6Sn_5. Kepler et al. first reported in-situ X-ray diffraction measurements of the reversible two-step reaction between Li and Cu_6Sn_5 [4], soon followed by Larcher et al. [5]. The stoichiometry of the intermediate lithiated phase, Li_2CuSn, was found to be close to $Li_{2.17}CuSn_{0.83}$ after

* Corresponding author. Department of Physics and Atmospheric Science, Dalhousie University, P.O. Box 15000, Halifax, Nova Scotia B3H 4R2, Canada. Tel.: +1 902 494 2394; fax: +1 902 494 5191.
E-mail addresses: jsthorne@dal.ca (J.S. Thorne), dunlap@fizz.phys.dal.ca (R.A. Dunlap).

0378-7753/$ – see front matter © 2012 Elsevier B.V. All rights reserved.
doi:10.1016/j.jpowsour.2012.05.067

lithiation to 0.2 V [6], followed by lithiation to form $Li_{4.4}Sn$ near 0 V. This work was followed by the investigation of a number of electrodeposited Sn–Cu-based materials [7–12]. These materials suffered from large irreversible capacity loss on the first cycle (possibly due in part to the formation of Sn-oxides in starting materials [13]), low Coulombic efficiencies and high capacity loss within the first 50 cycles. These effects can be attributed to numerous factors including the large stress/strain resulting from the high volume changes in large crystallites and SEI formation.

It is believed that nanostructured materials are best suited for high volume expansion alloys [1–3] and some progress has been made in the development of such materials in the Cu–Sn system. Some success has been achieved using chemical methods to create nanosized Sn–Cu grains [14]. Broadened X-ray diffraction peaks, suggesting relatively small crystallite size, have been observed for Cu–Sn alloys after >100 h of mechanical milling [15]. Nanoscale "core–shell" carbon-coated Cu–Sn alloys have been created using an in-situ polymerization technique with promising results (i.e. 400 mAh g^{-1} after 50 cycles), but these still suffer from a large irreversible capacity [16].

One possible way to reduce grain size in Sn–TM alloys is to add carbon, as has been observed for other systems [2,17–19]. We have previously reported an investigation of the Sn–Cu–C system prepared by combinatorial sputtering [19] and have shown that alloys with compositions containing Cu_6Sn_5 + C have superior electrochemical characteristics in comparison to other Cu_6Sn_5-based electrodes reported in the literature.

An alloy of Cu_6Sn_5 with 40 atomic percent carbon, shown to have good performance in combinatorial sputtering studies. While sputtering is not an economically viable method for producing commercial battery electrode materials, it is the most efficient method for high-throughput screening of different compositions. The ability of preparing materials by a more economical and scaleable method such as milling is essential for commercialization. An understanding of the relationship between properties of sputtered samples and those prepared by scaleable methods is necessary for the application of newly developed materials. In the present work, this approach has been taken and an alloy of composition $Sn_{27}Cu_{33}C_{40}$ has been prepared by milling methods and compared to sputtered samples of similar composition.

While commercially viable electrode materials are often more complex than those studied in the present work, an understanding of the basic physics of the behavior of simpler materials is helpful in interpreting studies of other related systems. The Cu–Sn- and Cu–Sn–C-based materials studied here are an example where the understanding gained is applicable to the interpretation of studies of commercially viable electrode materials (e.g. see recent publications such as [20]). Similar assessments have been made using other transition metals in Sn–TM–C, where combinatorial investigations have been made [2,17] followed by mechanical milling of specific compositions [3]. This, in combination with past work on Sn–Cu–C [19,21,22], provides a detailed picture of the viability of Cu_6Sn_5-based electrodes, and can be used as a basis for understanding other amorphous alloy materials for use as negative electrode materials.

2. Experimental

$Sn_{27}Cu_{33}C_{40}$ alloy was prepared by mechanical milling of stoichiometric amounts of Cu_6Sn_5 alloy (arc melted from the elements, Alfa Aesar, 99.5%) and graphite (Fluka, purum) in an argon atmosphere. Two alloys of similar composition were prepared by magnetron sputtering using a modified Corona Vacuum Systems V3-T deposition system. The sputtering chamber reached a base pressure of less than 3×10^{-7} Torr before sputtering was started and was maintained at a pressure of 2.0 mTorr of argon during the deposition. Cu targets 5.08 cm in diameter were cut from a 0.635 cm thick Cu plate (99.9% pure). Two carbon sputtering targets (5.08 cm diameter, 0.635 cm thick, and 99.999% pure) were obtained from Kurt J. Lesker Co. (Clairton, PA). A Sn sputtering target which was 5.08 cm diameter and 0.330 cm thick (99.85% pure) was cut from a Sn plate obtained from Alfa Aesar (Ward Hill, MA). All targets were mounted on 0.318 cm thick copper backing plates using SilverTech PT-1 silver epoxy from Williams Advanced Materials.

The sputtering substrate tables were covered with a large area of 25 μm thick polystyrene film and a small Si [100] wafer piece. The substrate table rotation speed was ~15 rpm to ensure intimate mixing of Sn, Cu and C on the atomic scale. Sputtering parameters for an identical sample are listed in previous work [22]. The materials sputtered on polystyrene were recovered by repeated rinsing and dissolving of the polystyrene in toluene followed by acetone. The obtained powders were rinsed at least six times before drying and collection. The resulting Sn–Cu–C nanostructured alloys were then ground by hand into a fine powder using a mortar and pestle over a period of 30–60 min. X-ray diffraction patterns of the recovered powders verified that grain aggregation did not occur over the course of the treatment as a result of the relatively small activation energy associated with crystallization [21].

All electrodes were prepared in a slurry mixture with 80% by weight Cu_6Sn_5 + C material, 12% Super-S carbon black (MMM Carbon, Belgium) and 8% lithium polyacrylate (Li-PAA, 11% solution in water) binder. A small amount of extra water was added, if necessary, to produce the correct viscosity for coating. The electrode material, carbon black and binder solution were mixed using a Mazerustar planetary mixer/deaerator. The slurries were spread on Cu foil with a notch bar and dried at 80–90 °C for 1–2 h. 1.267 cm^2 circular electrodes were then punched from the coating and these had an active mass of 0.00493 g cm^{-2} for the milled sample and 0.00215 g cm^{-2} for the sputtered samples. All cells contained an electrolyte consisting of 1 M $LiPF_6$ (Stella, Japan) dissolved in 1:2 EC:DEC (Novolyte Technologies, USA) with 10% by weight monofluoroethylene carbonate (FEC) (Fujian Chuang Xin, China). Choi et al. [23] showed that the addition of FEC to the electrolyte improves capacity retention and Coulombic efficiency for a silicon thin film electrode. 2325 size coin-type cells with two Celgard 2300 separators and a lithium foil counter/reference electrode were assembled in an Ar-filled glovebox.

The same electrochemical testing protocol was used for all cells. After assembly, coin cells were discharged from open circuit (near 2.7 V) to 0.005 V. The potential was then increased again to 2.5 V. This was done for a total of two cycles at a calculated C/10 rate, assuming a 700 mAh g^{-1} as the theoretical capacity as calculated assuming 4.4 Li/Sn and 0.5 Li/C [2]. After the first two cycles, cells were cycled between 0.005 and 1.2 V at a calculated C/5 rate for the remainder of the test. For cells with a specific capacity of 400 mAh g^{-1}, the actual rate was approximately C/2.9 or approximately 0.297 mA cm^{-2} for the sputtered sample and 0.680 mA cm^{-2} for the milled sample.

XRD measurements were performed using an INEL CPS120 curved position-sensitive detector coupled to an X-ray generator equipped with a Cu target X-ray tube. A monochromator in the incident beam path limited the wavelengths striking the sample to Cu-K_α radiation (λ = 1.54 Å). The detector measures the entire diffraction pattern between scattering angles of 6° and 120° at once using a 2400-s dwell time.

Electron microprobe measurements were made using a JEOL JXA-8200 Superprobe to verify that the intended composition was achieved for the sputtered samples. The sputtered samples were found to have compositions $Sn_{27}Cu_{31}C_{42}$ and $Sn_{26}Cu_{31}C_{43}$. Room

temperature ^{119}Sn Mössbauer effect measurements were made using a Wissel System II constant acceleration spectrometer equipped with $Ca^{119m}SnO_3$ source. Center shifts are referenced to $CaSnO_3$.

3. Results and discussion

Fig. 1 shows a comparison of the XRD patterns collected for the mechanically milled $Sn_{27}Cu_{33}C_{40}$ (top panel) and the sputtered $Sn_{27}Cu_{31}C_{42}$ (bottom panel). The mechanically milled sample shows broadened peaks which closely match to hexagonal Cu_6Sn_5 with additional background noticed between $2\theta = 25–45°$ which has not previously been observed in Cu_6Sn_5 samples. The grain size of the mechanically milled sample was estimated by the Scherrer equation to be approximately 16 nm.

The X-ray diffraction pattern for the sputtered $Sn_{27}Cu_{31}C_{42}$ sample as shown in the bottom panel of Fig. 1 was observed to have two broadened humps centered near $2\theta = 30°$ and 43°. Amorphization of this composition is due to grain size reduction effects from the addition of C. This has also been observed for other sputtered Sn–TM–C alloy systems [2,17,18] and results from the inability of Sn and transition metal atoms to diffuse to form well-ordered crystalline phases in the presence of substantial amounts of C. This is primarily due to the intimate intermixing of C with Sn and the TM during the sputtering process. In previous studies of combinatorial Cu_6Sn_5 + C films, the ratio of the 30° and 43° X-ray diffraction peak areas is approximately constant as the amount of carbon increases for amorphous samples, but has a strong dependence on the ratio of Sn to Cu. Different peak intensity ratios may be caused by different proportions of Sn–Sn (30° peak) and Sn–Cu or Cu–Cu (43° peak) near-neighbor correlations in the nanostructured phase, as has been shown for other Sn–TM amorphous alloys [24]. Using the Scherrer equation to estimate the grain size of the amorphous/nanostructured Cu_6Sn_5 + C samples does not give meaningful results [21].

Fig. 2 shows a comparison of the Mössbauer spectra collected from samples prepared using the two methods. The mechanically

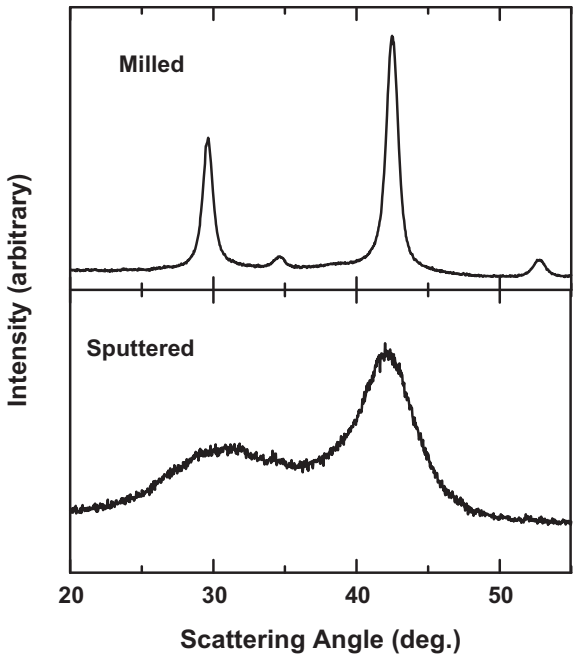

Fig. 1. XRD patterns of mechanically milled $Sn_{27}Cu_{33}C_{40}$ (top panel) and sputtered $Sn_{27}Cu_{31}C_{42}$ (bottom panel) samples.

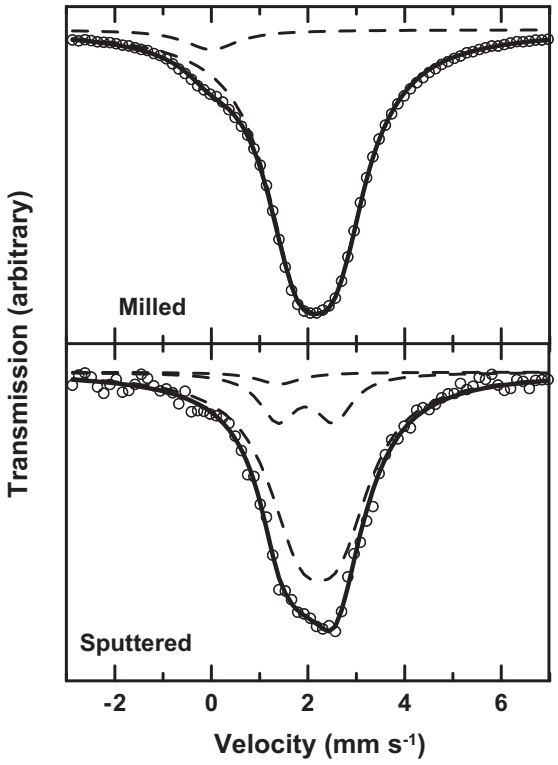

Fig. 2. Mössbauer spectra of mechanically milled $Sn_{27}Cu_{33}C_{40}$ (top panel) and sputtered $Sn_{27}Cu_{31}C_{42}$ (bottom panel) samples.

milled $Sn_{27}Cu_{33}C_{40}$ spectrum was fit with two sites having the following parameter values [relative component, area, center shift (CS), quadrupole splitting (QS)]: [Site 1, 95.6%, +2.19 mm s^{-1}, 0.81 mm s^{-1}], [Site 2, 4.4%, 0.0 mm s^{-1}]. Site 2 was a singlet and therefore had no QS and corresponds to a small amount of SnO_2 formed in the sample during the alloying process. The parameter values for site 1 are similar to those expected from well-ordered hexagonal Cu_6Sn_5, if fit with a single site [19,25]. However, the mechanically alloyed Cu_6Sn_5 cannot be fit with the three-site model which describes the three unique Sn sites found in well-ordered Cu_6Sn_5 [6]. This may be a result of a high degree of atomic disorder in the hexagonal phase and/or the relatively small grain size compared to bulk Cu_6Sn_5 samples. A relatively high surface to volume ratio may also be a contributing factor in the departure from bulk properties.

The parameter values used for the sputtered $Sn_{27}Cu_{31}C_{42}$ sample that gives the best fit are as follows: [Site 1, 81.5%, +2.23 mm s^{-1}, 0.81 mm s^{-1}], [Site 2, 16.0%, +1.95 mm s^{-1}, 1.16 mm s^{-1}], and [Site 3, 2.5%, +1.43 mm s^{-1}]. Site 3 was a singlet and therefore had no QS. No SnO_2 was detected in the sputtered sample. A comparison of these parameters with the results in Ref. [19] indicates that the values of sites 1–3 are close to those expected for this composition, with the exception of the relative areas which change with ageing time. This time-dependent change in peak area is due to the slow spontaneous crystallization of these samples at room temperature as reported in past work [21]. The sputtered powder was incorporated into electrochemical cells more than 30 days after the production of the film, and was additionally subject to treatment as described in the Experimental section. This, along with discussions presented in previous work [21], indicates that the variations in the relative areas are not necessarily unexpected.

The site 1 parameters for the sputtered sample are similar to those seen for the milled sample. This site is associated with Sn that

has a similar environment to the Sn in Cu_6Sn_5. Site 2 corresponds to Sn that has largely Cu nearest neighbors. Site 3 is attributed to Sn with C nearest neighbors [19]. The presence of site 2 and site 3, as described in previous work [19], reflects the much higher degree of atomic disorder and intermixing of atoms in the sputtered sample. The broad distribution of Sn environments is contrasted with crystalline samples containing a Cu:Sn ratio of 6:5 for which the crystalline Sn–Cu phase can be fit reasonably well by a single site. This is indicative of a narrower distribution of Sn environments in crystalline samples. Site 1 has hyperfine parameters that are similar to those of well-ordered single phase Cu_6Sn_5, which has an average center shift near +2.2 mm s^{-1} and quadrupole splitting near 0.7 mm s^{-1} [6,25]. Cu_6Sn_5-like phases have also been reported with center shifts near +2.10 mm s^{-1} and quadrupole splittings near 1.00 mm s^{-1} [26]. In general, the CS depends on the Sn:Cu ratio when Sn is surrounded by Cu, where increasing CS corresponds to Sn with increasingly Sn-rich environments [19].

Fig. 3 shows a comparison of the differential capacity (dQ/dV) as a function of voltage for the milled and sputtered samples as indicated during the first cycle. Fig. 4 shows a comparison of the voltage as a function of capacity for the milled and sputtered samples. The milled sample shows a striking similarity to bulk Cu_6Sn_5. Voltage plateaus are present near 0.35 V and 0.1 V during discharge (lithiation) in this work and correspond to the following two reactions, respectively

$$4.4Li + CuSn \rightarrow 2.4Li + Li_2CuSn \rightarrow Li_{4.4}Sn + Cu \quad (1)$$

as previously described with in-situ XRD for bulk Cu_6Sn_5 [4,5]. During charge (delithiation), the same features corresponding to the two reactions are seen near 0.8 V and 0.5 V respectively, however the peaks in the differential capacity are broader.

In bulk Cu_6Sn_5, the sloping and broadening of features of the low voltage charge plateau were explained by the formation of $Li_{4.4-x}Sn$ in a single phase region, accompanied with the kinetically hindered conversion of this phase to Li_2CuSn according to the reactions [5]:

$$Li_{4.4}Sn \rightarrow Li_{4.4-x}Sn + xLi, \quad (2)$$

$$Li_{4.4-x}Sn + Cu \rightarrow Li_2CuSn + (2.4 - x)Li. \quad (3)$$

At voltages above 0.5 V, during delithiation, the formation of Li_2CuSn is followed by a gradual sloping of the voltage curve. The onset of this feature was suggested to correspond to [5]:

$$Li_2CuSn \rightarrow Li_{2-x}CuSn + xLi \text{ for } 0 < x < 1. \quad (4)$$

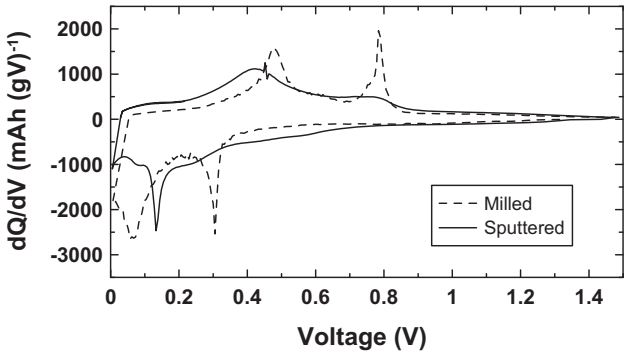

Fig. 3. Differential capacity (dQ/dV) as a function of voltage for mechanically milled $Sn_{27}Cu_{33}C_{40}$ cell #1 (dashed line) and sputtered $Sn_{27}Cu_{31}C_{42}$ cell #1 (solid line) during the first cycle.

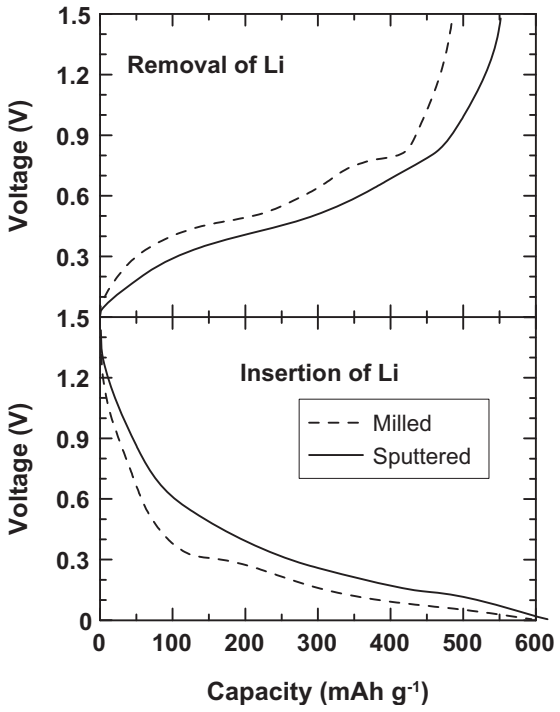

Fig. 4. Voltage as a function of capacity for the first delithiation (top panel) and lithiation (bottom panel) for mechanically milled (dashed line) and sputtered (solid line) samples corresponding to those in Fig. 3.

indicative of the existence of single phase $Li_{2-x}CuSn$ for given values of x. This is immediately followed by a voltage plateau corresponding to the two-phase reaction

$$Li_{2-x}CuSn \rightarrow CuSn + (2 - x)Li \text{ for } x > 1, \quad (5)$$

in which the partially delithiated $Li_{2-x}CuSn$ is in co-existence with CuSn. This plateau is characterized by a sharp differential capacity peak, characteristic of a two-phase region.

Broadening of the high voltage differential capacity peak during delithiation of the milled sample in Fig. 3 could be the result of small grain size effects and/or the presence of single phase Li_xCuSn or Li_xSn. These are not mutually exclusive effects. In-situ work on the milled samples would be required to determine the mechanism involved.

When compared to bulk Cu_6Sn_5 from Larcher et al. [5], the milled and the sputtered Cu_6Sn_5 + C samples in Figs. 3 and 4 show a progressive broadening of the differential capacity peaks when going from bulk to milled to sputtered samples. This corresponds to a decreasing grain size. The first discharge seen in the amorphous sample bears no similarity to that for milled Cu_6Sn_5 + C and bulk Cu_6Sn_5. This is the result of the dramatic reduction in grain size in the sputtered sample [2,3,17] in which there is intimate atomic mixing of Sn, Cu and C. The smooth sloping lithiation is the result of the uniform and gradual reaction of Li with the Sn in the Sn–Cu–C mixture. The effect is similar to amorphous Sn–Co–C [2,27]. Atomic intermixing in the sputtered sample is also likely the cause of a single phase Li_xCuSn, Li_xSn or an intermediate Li_xCu_ySn mixture having $2 < x < 4.4$ and $0 < y < 1$ [19] as lithium is inserted and removed.

In contrast, the differential capacity during charge for the sputtered sample has striking similarity, albeit having broader peaks, to the charge curve of the milled sample, suggesting a similar mechanism during delithiation.

Fig. 5 shows a comparison of the cycling performance of the milled and sputtered samples. Shown are three cells for the milled $Sn_{27}Cu_{33}C_{40}$, two cells for sputtered $Sn_{27}Cu_{31}C_{42}$, and two cells for sputtered $Sn_{26}Cu_{31}C_{43}$. Cells made for the milled sample are well reproduced for the first 50 cycles. All cells containing the sputtered samples had similar performance for 90 cycles or more. The addition of carbon in milled and sputtered samples results in superior capacity retention compared to bulk crystalline Cu_6Sn_5, electrodeposited Cu_6Sn_5 and other Cu_6Sn_5-based samples reported in the literature [3,7–16]. All samples have reversible capacities near 400 mAh g^{-1} after 10–20 cycles. The sputtered samples retain capacities near 400–420 mAh g^{-1} for 80 cycles, after which small capacity loss begins to become evident. The milled cells begin to show significant capacity loss after about 40 cycles. The improved performance of these samples compared to crystalline Cu_6Sn_5 is likely due to the addition of carbon, leading to a reduced Cu_6Sn_5 grain size. The reduced grain size may also responsible for the formation of single phase Li_x(Cu–Sn) and Li_xSn compositions during charge, an effect which has been described in previous in-situ studies on the amorphous $Sn_{27}Cu_{31}C_{42}$ [22]. This represents a departure from the abrupt two-phase transitions seen in bulk Cu_6Sn_5 [5]. Additionally the presence of pure carbon results in a smaller overall particle volume expansion than the pure Cu_6Sn_5 alloy [2,3,17,28].

Fig. 6 shows a comparison of the evolution in dQ/dV as a function of V for milled cell #1 and sputtered $Sn_{27}Cu_{31}C_{42}$ cell #1 cycling at about C/2.9 rate. In the milled sample, the peaks during discharge corresponding to reaction (1) broaden during cycling. During charge, the peak associated with the delithiation of Sn (reaction (3)) also broadens. This is likely due to the reduction in the grain size of the Sn–Cu regions during cycling. The reactions associated with these low voltage peaks are thought to have some single phase character when grain sizes are reduced, as peak broadening in this region of the voltage curve is observed even for bulk samples [5]. This would lead to the rapid broadening of these peaks if grain size reduction occurs during cycling. At the same time, the high voltage peak during charge, changes little as cycling progresses. This peak does not broaden in bulk samples as do the lower voltage peaks [5], indicating, the two-phase reaction associated with this peak (reaction (5)) is less dependent on grain size. It is even possible that the presence of this two-phase region may only depend on the Sn–Cu grain size, and not on its crystallinity.

Sharp peaks in differential capacity, as seen here for the high voltage two-phase region of the charge plateau, can cause internal stress in the particle and lead to particle fracture, electrical disconnection and capacity loss. This is the likely cause of the early capacity loss observed for this material. Indeed, internal strain and particle fracture due to two-phase regions encountered during cycling is also likely the cause of the reduction in grain size observed during cycling.

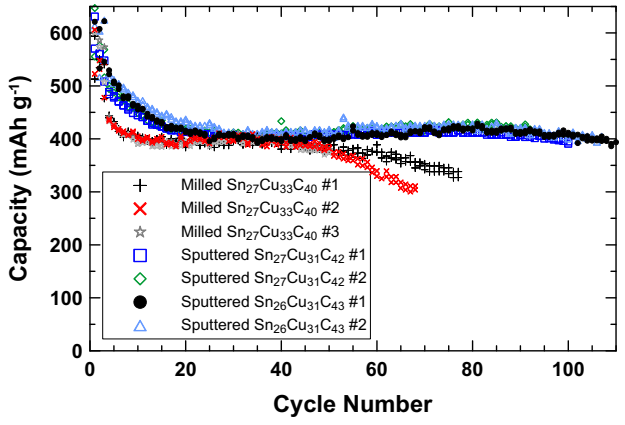

Fig. 5. Specific capacity as a function of cycle number for cells #1–3 containing the mechanically milled sample and cells #1–2 for each of the sputtered samples, as labeled.

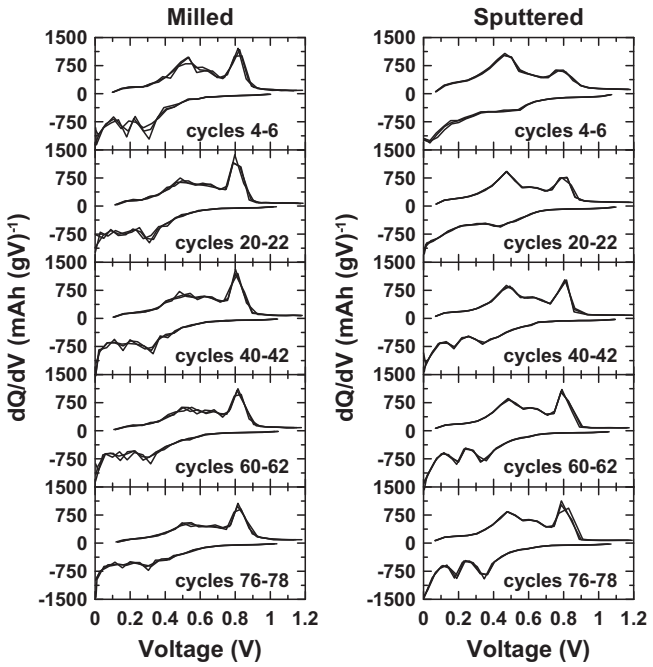

Fig. 6. A comparison of differential capacity (dQ/dV) as a function of voltage for the mechanically milled $Sn_{27}Cu_{33}C_{40}$ cell #1 (left) and sputtered $Sn_{27}Cu_{31}C_{42}$ cell #1 (right) samples during selected cycles.

The relatively amorphous sputtered sample is in stark contrast and an opposite effect appears to be occurring. During cycling, the high voltage peak during charge is first seen to sharpen. This likely indicates aggregation of Sn–Cu regions in the alloy. Initially Sn–Cu regions were too small to support two-phase behavior, due to small size effects [22,29]. As Sn–Cu aggregation occurs, two-phase behavior is first seen to emerge in the high voltage charge plateau. Upon further cycling the alloy is seen to crystallize as the aggregated Sn–Cu regions can reorganize. Finally, by cycle 78 the differential capacity of the sputtered alloy looks similar to that of the first few cycles of the milled alloy. It is likely that the sputtered alloy will now lose capacity due to particle fracture in a similar manner as the milled alloy. This fade can be seen to begin after cycle 80 in the sputtered sample in Fig. 5. Further studies are needed to verify long-term cycling behavior.

In past work, Cu_6Sn_5 grain growth was shown to occur at room temperature for amorphous sputtered Cu_6Sn_5 + C samples [21] which implies that the activation energy associated with crystallization is relatively small. A consequence of the low activation energy is seen here in the electrochemistry with the progressive formation of Cu_6Sn_5 or a Cu_6Sn_5-like structure with cycling. The Cu_6Sn_5 grain reformation necessarily occurs during charge. The crystallization and grain growth process must occur when Li is being removed and pure regions of Cu–Sn–C are being restored. At this stage, there is always a tendency for hexagonal Cu_6Sn_5 to form spontaneously when Sn and Cu atoms are nearby [21] via a similar reaction to (5). This is likely the primary reason for the presence of the high voltage plateau seen on charge even in later cycles in the milled sample.

Fig. 7 shows a DSC trace of the milled $Sn_{27}Cu_{33}C_{40}$ and sputtered $Sn_{27}Cu_{31}C_{42}$ samples between temperatures of 30–400 °C.

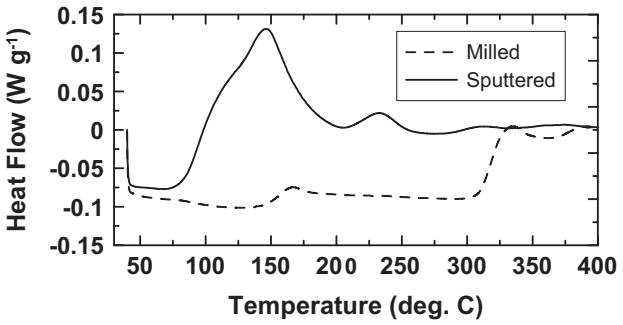

Fig. 7. DSC comparison of the milled sample with the sputtered amorphous/nanostructured $Sn_{27}Cu_{31}C_{42}$ at a heating rate of 10 °C min^{-1}.

Observed is a very broad exothermic feature in the sputtered sample centered near 150°C. This is likely associated with the crystallization of Cu_6Sn_5, as has been observed at room temperature [21] and here during the lithiation/delithiation of the sample. No significant exothermic features occur above 200 °C, as was also found with a temperature sweeps up to 600 °C. The milled sample has no significant feature in this range, which helps to confirm that the exothermic features in the sputtered sample are associated with crystallization. This is in stark contrast to amorphous $Sn_{30}Co_{30}C_{40}$, in which crystallization of the Sn–Co appears to occur at temperatures in excess of 350 °C [30]. Additionally, as no crystallization occurs below these temperatures, no significant effect was seen on the cycling capability of the Sn–Co–C at annealing temperatures below 300 °C [31]. This suggests that amorphous Cu_6Sn_5 + C alloys are more unstable towards metal aggregation, leading to more grain growth than Sn–Co–C alloys. This provides further clues to the reasons for the changes observed in dQ/dV for this material.

4. Conclusions

Cu_6Sn_5 + C alloys were prepared using sputtering and milling techniques. From the standpoint of capacity retention, stability and Coulombic efficiency, the alloys produced here have superior electrochemical performance compared to other Cu_6Sn_5-based alloys reported in the literature [3,5,7–16]. In amorphous $Sn_{27}Cu_{31}C_{42}$ and $Sn_{26}Cu_{31}C_{43}$, a capacity near 400 mAh g^{-1} was retained after 100 charge–discharge cycles, while for the milled $Sn_{27}Cu_{33}C_{40}$, a capacity over 300 mAh g^{-1} can be retained after 80 cycles. The addition of carbon is primarily responsible for the improvement. The positive effects are likely a result of a reduction of grain size and the additional buffering of Sn by regions of pure C, the extent of which is a function of the method of sample preparation.

Results presented here (and elsewhere) suggest that it may be difficult to produce Cu_6Sn_5 + C based materials that remain amorphous during cycling [3,7–16]. This is in contrast to Sn–Co–C and other Sn–TM–C materials [3]. Apart from the room temperature crystallization of amorphous Cu_6Sn_5 + C previously reported which can occur over periods in excess of one year [21], crystallization of the Cu_6Sn_5 also appears to occur in similar Cu_6Sn_5 + C amorphous materials during the insertion and removal of Li [19]. DSC supports the conclusion that metal aggregation and crystallization of Cu_6Sn_5 in a Cu_6Sn_5 + C mixture are associated with a relatively low activation energy (i.e., in comparison to SnCo + C [30]). This has implications for the practical application of Cu_6Sn_5 + C composites.

Acknowledgements

The authors acknowledge funding from NSERC and 3M Canada, Co. under the auspices of the Industrial Research Chairs Program. We also acknowledge the support of the Canada Foundation for Innovation, the Atlantic Innovation Fund and other partners that fund the Facilities for Materials Characterization managed by the Institute for Research in Materials.

References

[1] M. Winter, J.O. Besenhard, Electrochim. Acta 45 (1999) 31–50.
[2] J.R. Dahn, R.E. Mar, A. Abouzeid, J. Electrochem. Soc. 153 (2006) A361–A365.
[3] P.P. Ferguson, M.L. Martine, A.E. George, J.R. Dahn, J. Power Sources 194 (2009) 794–800.
[4] K.D. Kepler, J.T. Vaughey, M.M. Thackeray, Electrochem. Solid-State Lett. 2 (1999) 307–309.
[5] D. Larcher, L.Y. Beaulieu, D.D. MacNeil, J.R. Dahn, J. Electrochem. Soc. 147 (2000) 1658–1663.
[6] E. Nördström, S. Sharma, E. Sjöstedt, L. Fransson, L. Häggström, L. Nordström, K. Edström, Hyperfine Interact. 136 (2001) 555–560.
[7] S.D. Beattie, J.R. Dahn, J. Electrochem. Soc. 150 (2003) A894–A898.
[8] N. Tamura, R. Ohshita, M. Fujimoto, S. Fujitani, M. Karmino, I. Yonezu, J. Power Sources 107 (2002) 48–55.
[9] L. Trahey, J.T. Vaughey, H.H. Kung, M.M. Thackeray, J. Electrochem. Soc. 156 (2009) A385–A389.
[10] W. Zhou, L. Liu, P. Wu, Intermetallics 18 (2010) 922–928.
[11] J. Park, J. Eom, H. Kwong, Electrochim. Acta 55 (2010) 1825–1828.
[12] W. Pu, X. He, J. Ren, C. Wan, C. Jiang, Electrochim. Acta 50 (2005) 4140–4145.
[13] I.A. Courtney, J.R. Dahn, J. Electrochem. Soc. 144 (1997) 2045–2052.
[14] J. Wolfenstine, S. Campos, D. Foster, J. Read, W.K. Behl, J. Power Sources 109 (2002) 230–233.
[15] G.X. Wang, L. Sun, D.H. Bradhurst, S.X. Dou, H.K. Liu, J. Alloys Compd. 299 (2000) L12–L15.
[16] W. Cui, F. Li, H. Liu, C. Wang, Y. Xia, J. Mater. Chem. 19 (2009) 7202–7207.
[17] A.D.W. Todd, R.E. Mar, J.R. Dahn, J. Electrochem. Soc. 154 (2007) A597–A604.
[18] A.D.W. Todd, P.P. Ferguson, J.G. Barker, M.D. Fleischauer, J.R. Dahn, J. Electrochem. Soc. 156 (2009) A1034–A1040.
[19] J.S. Thorne, R.J. Sanderson, J.R. Dahn, R.A. Dunlap, J. Electrochem. Soc. 157 (2010) A1085–A1091.
[20] D. Applestone, A. Manthiram, RSC Adv. 2 (2012) 5411–5417.
[21] J.S. Thorne, J.R. Dahn, M.N. Obrovac, R.A. Dunlap, J. Alloys Compd. 509 (2011) 6705–6710.
[22] J.S. Thorne, J.R. Dahn, M.N. Obrovac, R.A. Dunlap, J. Electrochem. Soc. 158 (2011) A1328–A1334.
[23] N.-S. Choi, K.H. Yew, K.Y. Lee, M. Sung, Ho Kim, S.-S. Kim, J. Power Sources 161 (2006) 1254–1259.
[24] J.F. Geny, G. Marchal, P. Mangin, C. Janot, M. Piecuch, Phys. Rev. B 25 (1982) 7449–7466.
[25] L. Fransson, E. Nordström, K. Edström, L. Häggström, J.T. Vaughey, M.M. Thackeray, J. Electrochem. Soc. 149 (2002) A736–A742.
[26] A. Vértes, J. Jaen, L. Kiss, E.V. Shepelewa, Hyperfine Interact. 28 (1986) 1079–1081.
[27] P.P. Ferguson, R.A. Dunlap, J.R. Dahn, J. Electrochem. Soc. 157 (2010) A326–A332.
[28] Wei-Jun Zhang, J. Power Sources 196 (2011) 13–24.
[29] M.N. Obrovac, J.R. Dahn, Phys. Rev. B 61 (2000) 6713–6719.
[30] J.S. Thorne, P.P. Ferguson, R.A. Dunlap, J.R. Dahn, J. Alloys Compd. 472 (2009) 390–394.
[31] P.P. Ferguson, J.R. Dahn, Electrochem. Solid-State Lett. 11 (2008) A187–A189.